https://doi.org/10.5194/egusphere-2025-1569
Preprint. Discussion started: 16 April 2025

Mapping seasonal nitric acid (HNO_3) patterns in the extratropics with nadir-viewing infrared sounders – a retrieval perspective

Nadia Smith[1], Michelle L. Santee[2], Christopher D. Barnet[1*]

[1]Science and Technology Corporation, Columbia, Maryland, USA
[2]Jet Propulsion Laboratory, California Institute of Technology, Pasadena, California, USA
* Retired

Correspondence to: Nadia Smith (nsmith@stcnet.com)

Abstract.

With this paper, we aim to shed light on the extent to which nadir-viewing hyperspectral infrared (IR) sounders can support the study of stratospheric chemical processes and ozone loss in the extratropics. We use CLIMCAPS (Community Long-term Infrared Microwave Combined Atmospheric Processing System) retrievals from JPSS-1 (Joint Polar Satellite System) CrIS (Cross-track Infrared Sounder) measurements as the baseline case. CLIMCAPS retrieves a suite of Earth system variables that includes atmospheric temperature (T_{air}), water vapor (H_2O_{vap}), carbon dioxide (CO_2), carbon monoxide (CO), methane (CH_4), ozone (O_3), and nitric acid (HNO_3). Unlike the Rodgers (2000) Optimal Estimation (OE) retrieval approach, CLIMCAPS regularizes its Bayesian inverse solution dynamically using singular value decomposition (SVD) at run-time to separate measurement signal from noise. We illustrate how the CLIMCAPS approach enables stable retrievals of stratospheric HNO_3 under highly variable conditions, allowing characterization of seasonal patterns. Nitric acid is typically used as an indicator species for heterogeneous chemical processing inside the winter stratospheric polar vortices. This paper summarizes our diagnostic evaluation of CLIMCAPS observing capability during the Northern Hemisphere winter of 2019/2020. We contrast CLIMCAPS HNO_3 retrievals with those from the limb-viewing MLS (Microwave Limb Sounder) to illustrate the capability of this retrieval approach and lay the foundation for in-depth validation studies in future.

1 Introduction

Measurements of HNO_3 help explain O_3 chemical processes, especially in the extratropical stratosphere, where seasonal O_3 holes form to the detriment of life on Earth. Instruments on Earth-orbiting satellites provide the bulk of the observations necessary to monitor O_3 loss. Two types of modern-era space-based instruments have the ability to observe stratospheric gases, namely limb-viewing sounders, such as MLS (Microwave Limb Sounder; Waters et al., 2006), and nadir-viewing sounders, such as IASI (Infrared Atmospheric Sounding Interferometer; Chalon et al., 2017). The most basic distinction one can draw as far as stratospheric observation goes is as follows: limb sounders have higher vertical resolution but more limited spatial coverage with narrow instrument swath widths, while nadir sounders have lower vertical resolution yet more extensive spatial

https://doi.org/10.5194/egusphere-2025-1569
Preprint. Discussion started: 16 April 2025

coverage with much wider swath widths. Compared to MLS, the limited vertical sensitivity of IR sounders to HNO_3 prohibits the observation of multiple stratospheric layers, which can impede their ability to observe smaller, less predictable events. MLS was launched on the National Aeronautics Space Administration (NASA) Earth Orbiting System (EOS) Aura satellite in 2004. Two decades later, MLS remains unmatched in its ability to measure the chemical state of the atmosphere, from the upper troposphere to the mesosphere. In fact, MLS observations of atmospheric chemistry (15 species in total) have transformed our understanding of stratospheric processes. In contrast, IASI instruments – like all nadir sounders – measure the atmosphere from the boundary layer to the top of atmosphere (TOA) in wide swaths (~2000 km) from pole to pole. But their orbital configuration is not the only distinction to highlight. IASI is an infrared (IR) sounder and, unlike microwave sounders such as MLS, cannot measure the atmospheric state through clouds. Moreover, IASI is sensitive to a smaller number of chemical species. However, despite its scientific significance, MLS is the only instrument of its kind in operational orbit, and its record of stratospheric observations will end once Aura is decommissioned within the next couple of years. IASI, on the other hand, is one of many IR sounders in space and well supported with plans to continue measuring the atmosphere for the next two decades. A detailed comparison is beyond the scope of this paper, but such a basic distinction serves the purpose of our work described here.

While MLS retrievals of HNO_3 have been critically important to understanding and modelling stratospheric processes (e.g., Brakebusch et al., 2013; Santee et al., 2008), the use of IASI HNO_3 retrievals has not been as widespread. And for those studies that do exist, the IASI HNO_3 product is presented as a total column quantity (troposphere + stratosphere) in demonstrations that largely avoid the Arctic region, where vortices are both smaller and shorter-lived than those in the Antarctic. This paper presents the first assessment of HNO_3 retrievals from the Cross-track Infrared Sounder (CrIS; Glumb et al., 2002; Strow et al., 2013) with a methodology that allows the separation of tropospheric and stratospheric HNO_3 concentrations.

As stated earlier, IASI is one of many nadir-IR sounders in space. The Atmospheric InfraRed Sounder (AIRS) initiated the modern era of IR sounding capability when it was launched in 2002 on Aqua (Aumann et al., 2003; Pagano et al., 2003) in a sun-synchronous orbit with ~1:30 am/pm equatorial crossing time. In 2011, CrIS was launched on the Suomi National Polar Partnership (SNPP) payload to continue the AIRS record with observations of the atmosphere at ~1:30 am/pm equatorial crossing time. CrIS has since been launched on a series of payloads, collectively known as the Joint Polar Satellite System series (JPSS+), with JPSS-1 in 2017, JPSS-2 in 2022, and two additional JPSS payloads planned in the next decade. Like IASI, CrIS is poised to continue its record well into the 2040s. Despite this long record, however, a science-quality HNO_3 product was largely absent for AIRS and CrIS until CLIMCAPS V2.1 (Community Long-term Infrared Microwave Combined Atmospheric Processing System) was released in 2018 (Smith and Barnet, 2023a). HNO_3 was never before considered a target variable in the suite retrieved from the heritage AIRS Level 2 retrieval system (Susskind et al., 2003), and it features in the NOAA-Unique Combined Atmospheric Product System (NUCAPS) suite only as an experimental by-product (Barnet et al., 2021). The full suite of CLIMCAPS V2.1 retrieval products includes atmospheric temperature (T_{air}), eight gaseous species (H_2O_{vap}, CO_2, O_3, N_2O, CH_4, HNO_3, CO and SO_2), as well as cloud and Earth surface properties (see Table 1 in Smith and

https://doi.org/10.5194/egusphere-2025-1569
Preprint. Discussion started: 16 April 2025

Barnet, 2023a). The Fast Optimal Retrieval on Layers for IASI (FORLI; Ronsmans et al., 2016), in contrast, retrieves only CO, O_3 and HNO_3. Analysis of the FORLI HNO_3 product for IASI, therefore, relies on estimates of stratospheric T_{air} from external sources, while the CLIMCAPS product from AIRS and CrIS provides coincident observations of T_{air} and HNO_3.

The overall goal of this paper is to demonstrate the degree to which the CLIMCAPS V2.1 HNO_3 product can be improved so that it may aid the study and monitoring of extratropical stratospheric O_3 in future. To this end, we have identified two objectives. The first objective is to test the sensitivity of the CLIMCAPS HNO_3 retrieval to two algorithm components, namely channel selection and Bayesian regularization. CLIMCAPS employs a dynamic regularization approach in its retrieval system by decomposing the Bayesian information content matrix into its component eigenfunctions. CLIMCAPS uses `Bmax` – an input variable – to calculate the signal-to-noise-ratio (SNR) threshold for determining which eigenfunctions to filter, damp or use unconstrained during signal inversion. We discuss `Bmax` in more detail later, and for a general overview of the CLIMCAPS retrieval approach we refer the reader to previous work (Smith and Barnet, 2019, 2020). The second objective is to demonstrate the effectiveness of CLIMCAPS eigenvalue decomposition in separating stratospheric HNO_3, from tropospheric HNO_3 and most known sources of noise in the spectral measurement. Stated differently, our objective is to identify which eigenfunction(s) to employ for the retrieval of stratospheric HNO_3 from hyperspectral nadir-IR measurements.

Being a nadir-IR product, CLIMCAPS HNO_3 will never match the quality of the HNO_3 product from MLS. In fact, when Aura is decommissioned, the scientific community will lose a critical source of up-to-date stratospheric observations from MLS. Our aim, therefore, is *not* to continue the MLS record with CLIMCAPS retrievals but, rather, to help fill this data gap until a next-generation space-based MLS-like observing capability is restored. We envisage that CLIMCAPS soundings could prove useful in monitoring polar processes with an HNO_3 product indicating polar stratospheric cloud (PSC) formation. Additionally, the day-to-day variations (relative changes) in CLIMCAPS HNO_3 abundances over the course of a season, as well as anomalies from a long-term climatology, might convey meaningful information even if the absolute magnitudes are biased. In this sense, observations from nadir-IR sounders may have a place alongside those from OMPS/LP (Ozone Mapping and Profiler Suite Limb Profiler; Flynn et al., 2006) to characterize future seasonal O_3 processes in the extratropical stratosphere (Wargan et al., 2020). OMPS/LP was first launched on SNPP and will continue on JPSS+ alongside CrIS. OMPS/LP is similar to MLS in that it makes high-vertical-resolution limb measurements, but instead at much shorter wavelengths in the ultraviolet (UV) to near-IR range. Unlike CrIS, OMPS/LP depends on reflected sunlight for all observations and lacks any sensitivity to stratospheric HNO_3. OMPS/LP primarily observes daytime PSCs, other aerosols, and O_3 in the upper troposphere/lower stratosphere (UTLS). Despite the benefits offered by its limb-viewing geometry, OMPS/LP has no ability to observe atmospheric conditions during the dark polar winters when stratospheric vortices typically form. This means that, without MLS, the future of stratospheric O_3 studies will depend on observations from an ensemble of sources, which may routinely include both CLIMCAPS and OMPS/LP soundings.

https://doi.org/10.5194/egusphere-2025-1569
Preprint. Discussion started: 16 April 2025

The CLIMCAPS V2.1 product is publicly available at NASA GES DISC (Goddard Earth Science Data and Information Service Center) for Aqua (2002–2016; Smith, 2019a), SNPP (2016–2018; Sounder SIPS and Barnet, 2020c) and JPSS-1 (2018–present; Smith, 2019b). Our work in this paper will determine the system upgrades for a future CLIMCAPS V3 release.

In Section 2, we present our scientific rationale. Section 3 outlines the CLIMCAPS retrieval approach, which we contrast with the Bayesian Optimal Estimation (OE) framework put forward by Rodgers (2000) that has been widely adopted in many retrieval systems, including FORLI and MLS. In practice, however, the implementation of Rodgers (2000) OE varies greatly as considerations are made for different instruments and target retrieval parameters. Needless to say, a detailed comparison of retrieval systems is beyond the scope of this paper, but by making this distinction between CLIMCAPS and the generalized Rodgers (2000) framework, we aim to clarify how the CLIMCAPS system design differs from this theoretical standard and thus allows the separation of tropospheric HNO_3 from stratospheric HNO_3 during measurement inversion. We present the results of our HNO_3 sensitivity analysis in Section 4, and we end with a demonstration of the seasonal evolution of HNO_3 in the lower stratosphere during the 2019/2020 Arctic winter. A qualitative comparison of HNO_3 retrievals from CLIMCAPS and MLS (Version 5) demonstrates some of the fundamental differences between these two observing systems and highlights how CLIMCAPS data products may contribute to stratospheric polar studies in future. We summarize our recommendations for future upgrades to the CLIMCAPS HNO_3 product in Section 5.

2 Scientific Rationale

The characterization and monitoring of chemical O_3 loss is one of the primary applications for satellite retrievals of stratospheric HNO_3. In short, HNO_3-containing and ice PSCs initiate the chemical reactions that lead to O_3 loss inside polar vortices (e.g., Solomon, 1999). In addition to playing a key role in the conversion of stratospheric chlorine from benign into reactive O_3-destroying forms, HNO_3 is also involved in the deactivation of chlorine into reservoir forms at the end of winter. Therefore, the degree of chemical O_3 loss within any given polar vortex depends on the temperature and the presence of HNO_3. If PSC particles grow large enough for efficient sedimentation, then HNO_3 can be removed irreversibly from parts of the lower stratosphere (known as denitrification). It is not just the absolute temperature but also the thermal history of an air parcel that affects the state of PSCs and thus the rate of denitrification (Lambert et al., 2016; Murphy and Gary, 1995; Toon et al., 1986). These are complex chemical processes that can be monitored only with an ensemble of observations covering the chemical (e.g., HNO_3, O_3) and physical (e.g., T_{air} and PSCs) state of the atmosphere.

Nadir-IR sounders measure HNO_3 with peak sensitivity in the lower stratosphere (30–90 hPa), which is also where PSCs mainly form (e.g., Tritscher et al., 2021). Moreover, AIRS, CrIS and IASI (all in low-Earth orbit) make their measurements in wide swaths (~2000 km) with polar crossings every ~90 min irrespective of sunlight. In other words, not only do nadir-IR sounders observe HNO_3 in the area of interest for O_3 monitoring, but they do so with the ability to generate full-cover maps, both daytime and nighttime. Ronsmans et al. (2018) illustrate this with global maps of FORLI HNO_3 retrievals.

https://doi.org/10.5194/egusphere-2025-1569
Preprint. Discussion started: 16 April 2025

In Figure 1, we highlight some of the CrIS spectral features to emphasize its sounding capability. CrIS measures the IR spectrum in three distinct bands: longwave IR (650–1095 cm^{-1}), midwave IR (1210–1750 cm^{-1}), and shortwave IR (2155–2550 cm^{-1}). We limit our focus in Figure 1 to the two CrIS bands that report significant sensitivity to HNO_3, namely the longwave and midwave bands. The absorption features in Figure 1 were calculated as the absolute difference in brightness temperature (delta-BT) [Kelvin] given a perturbation of the target variable. We used the Stand-alone AIRS Radiative Transfer Algorithm (SARTA; Strow et al., 2003a) to calculate these delta-BT spectra with a CLIMCAPS sounding (i.e., the full suite of retrieved variables) as the background atmospheric state. Each target variable was perturbed in the lower stratospheric pressure layers (30–90 hPa), while keeping its value in all other layers constant.

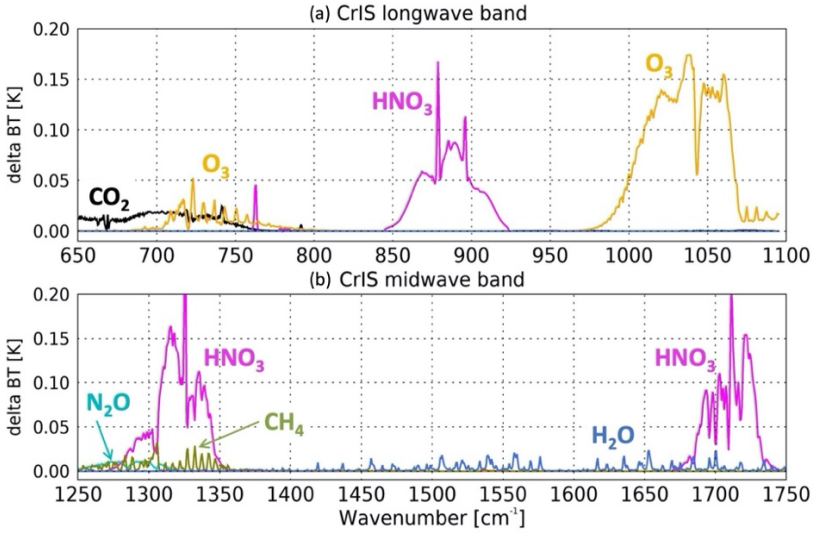

Figure 1: Lower stratospheric (30–90 hPa) trace gas absorption spectra as the absolute delta brightness temperature (BT) for six atmospheric gases active in the thermal IR as measured by CrIS in the (a) longwave (650–1095 cm^{-1}) and (b) midwave (1210–1750 cm^{-1}) bands. These delta-BT spectra were calculated using the SARTA forward model and CLIMCAPS L2 retrievals as state parameters on 2019/12/03 at [76.7°N, 124.1°E]. Each gas was perturbed by a fraction in the stated pressure layers as follows: H_2O_{vap} by 10%, O_3 by 10%, HNO_3 by 40%, CH_4 by 15%, N_2O by 5% and CO_2 by 1%. The CrIS shortwave IR band (2155–2550 cm^{-1}) is absent in this figure because neither O_3 nor HNO_3 are spectrally active in this spectral region.

Note the three distinct absorption signals for HNO_3 (centred about 890 cm^{-1}, 1325 cm^{-1} and 1725 cm^{-1}) and two for O_3 (centred about 725 cm^{-1} and 1025 cm^{-1}). Signals for HNO_3 and O_3 in the longwave band (Figure 1a) are in the spectral window regions (~850–900 cm^{-1} and 1000–1050 cm^{-1}, respectively), which means that these channels have strong sensitivity to the thermodynamic structure of the troposphere, i.e., clouds, surface emissivity and T_{air}. The HNO_3 signal centred at 1325 cm^{-1} in the midwave band is, in turn, weakly sensitive to lower stratospheric N_2O and CH_4. We, therefore, regard N_2O and CH_4 as spectral interference (or geophysical noise) in this HNO_3 band. Similarly, the HNO_3 signal centred at 1725 cm^{-1} has weak sensitivity to stratospheric H_2O_{vap}. Even though observations of H_2O_{vap} can be very useful in characterizing chemical

https://doi.org/10.5194/egusphere-2025-1569
Preprint. Discussion started: 16 April 2025

processing, the midwave IR band does not have sufficient sensitivity to stratospheric H_2O_{vap}, relative to all sources of signal and noise, to yield stable retrievals in this part of the atmosphere. Nadir IR sounders are primarily sensitive to tropospheric H_2O_{vap}, which CLIMCAPS retrieves with high accuracy (Smith and Barnet, 2020, 2023a). As far as O_3 goes, the stratospheric signal centred at 725 cm^{-1} is not only much weaker than the one centred at 1025 cm^{-1}, but it is also affected by CO_2 absorption. Even though CrIS is a nadir-viewing IR sounder with much lower vertical resolution than MLS, our aim with Figure 1 is to demonstrate the potential for optimizing CLIMCAPS HNO_3 and O_3 retrievals with respect to the number and spectral range of available IR channels.

3 Retrieval experiments and technical overview of CLIMCAPS

Here we describe the experimental setup for optimizing and characterizing CLIMCAPS HNO_3 retrievals. We give a generalized overview of the CLIMCAPS retrieval approach to clarify how we are able to separate stratospheric and tropospheric HNO_3, while simultaneously minimizing all known sources of geophysical noise in the longwave IR window region (~11μm).

CLIMCAPS also uses the SARTA forward model (Strow et al., 2003) in its physical Bayesian inversion of IR measurements. SARTA requires all input atmospheric state variables to be defined on 101 pressure levels (for T_{air}) and 100 pressure layers (for H_2O_{vap}, O_3, CH_4, CO, HNO_3, CO_2 and N_2O) in order to calculate top-of-atmosphere (TOA, ~0.01 hPa) radiances. But once those are calculated, CLIMCAPS solves the inverse solution for each target variable on a reduced set of pressure layers that are defined as trapezoidal shapes to account for pressure-layer correlation and a more accurate representation of measurement information content with respect to each target variable (Maddy and Barnet, 2008; Susskind et al., 2003). CLIMCAPS retrieves HNO_3 in eight pressure layers that Table 1 lists as the hinge points and effective mean values for each layer. The CLIMCAPS HNO_3 a priori estimate is the climatological profile developed by the Air Force Geophysical Laboratory (AFGL; Anderson et al., 1986) that SARTA also employs for its TOA radiance calculations. The AFGL HNO_3 profile represents a global average ranging between 1 and 0.01 ppb in the UTLS.

Table 1: Summary of the two CLIMCAPS HNO_3 algorithm components – `Bmax` and channel selection – tested in this study. Four different `Bmax` values and two different channel selections define five experimental setups in total, R1 – R5. The righthand column specifies the hinge points and effective mean values of the pressure layers on which CLIMCAPS retrieves HNO_3.

	`Bmax` (λ_c)	Wavenumbers of the channel subsets used in the HNO_3 retrievals [cm^{-1}]. All channels are centred in the IR window region (~11μm)	Retrieval pressure grid
R1	1.5 (0.44)	846.250, 847.500, 851.250, 855.625, 857.500, 858.125, 860.625, 861.875, 862.500, 867.500, 869.375, 873.125, 875.000, 876.875, 880.000, 881.875, 885.625, 893.125, 894.375, 895.625, 898.750, 900.000, 901.250, 902.500, 904.375, 907.500, 911.250, 912.500, 920.000 **[30 total]**	9 x Pressure hinge points of retrieval layers: [0.04, 9.51, 51.53, 77.24, 110.24, 170.08, 374.73, 477.96, 1042.23] hPa
R2	0.5 (4.00)	858.750, 859.375, 860.000, 860.625, 861.250, 861.875, 862.500, 863.125, 863.750, 864.375, 865.000, 865.625, 866.250, 866.875, 868.125, 868.750, 869.375, 870.000, 870.625, 871.250,	

https://doi.org/10.5194/egusphere-2025-1569
Preprint. Discussion started: 16 April 2025

R3	1.5 (0.44)	871.875, 872.500, 873.125, 873.750, 874.375, 875.000, 875.625, 876.250, 876.875, 877.500, 878.125, 878.750, 879.375, 880.000, 880.625, 881.250, 881.875, 882.500, 883.125, 883.750, 884.375, 885.000, 885.625, 886.250, 886.875, 887.500, 888.125, 888.750, 889.375, 890.000, 890.625, 891.250, 891.875, 892.500, 893.125, 893.750, 894.375, 895.000, 895.625, 896.250, 896.875, 897.500, 898.125, 898.750, 899.375, 900.000, 900.625, 901.250, 901.875, 902.500, 903.125, 903.750, 904.375, 905.000, 905.625, 906.250, 906.875, 907.500, 908.125, 908.750, 909.375, 910.000, 910.625, 911.250, 911.875, 912.500, 913.125, 913.750, 914.375, 915.000, 915.625, 916.250, 916.875, 917.500, 918.125, 918.750, 919.375, 920.000, 920.625, 921.250, 921.875, 922.500, 923.125, 923.750, 924.375, 925.000, 925.625, 926.250, 926.875, 927.500, 928.120 **[111 total]**	8 x Effective mean pressure values of retrieval layers: [1.31, 22.25, 58.52, 86.33, 129.64, 246.56, 407.27, 733.88] hPa
R4	2.5 (0.16)		
R5	10 (0.01)		

These HNO_3 layers follow the CLIMCAPS V2.1 definition and are the same layers used in the NUCAPS HNO_3 retrieval. Both CLIMCAPS and NUCAPS have their origins in the heritage AIRS retrieval system (Susskind et al., 2003) and share many algorithm components, as described in Berndt et al. (2023). Historically, HNO_3 was added to the NUCAPS retrieval sequence primarily to improve the T_{air} SNR (Figure 1 in Berndt et al., 2023 summarizes this step-wise approach). CLIMCAPS V2.1 takes a similar stepwise retrieval approach, as illustrated in Smith and Barnet (2023a). Figure 2 (rightmost panel) depicts the CLIMCAPS HNO_3 averaging kernels (AKs) on seven of the eight broad retrieval layers. At every retrieval footprint, CLIMCAPS calculates an AK matrix.

Table 1 lists the two experimental HNO_3 channel sets used here. Experimental run **R1** represents the operational CLIMCAPS V2.1 set-up with `Bmax` = 1.5 and a 30-channel subset selected from the longwave IR window band (850–920 cm^{-1}, or ~11 μm). The only difference between **R1** and the operational V2.1 product is that the forward model error spectrum (`RTAERR`) is set to zero in **R1**. As identified in Smith and Barnet (2024), the V2.1 `RTAERR` for the CLIMCAPS-CrIS retrieval configuration is too high relative to the CLIMCAPS-AIRS configuration, and we made the recommendation that a future CLIMCAPS V3 release should update the `RTAERR` accordingly. An overestimated `RTAERR` lowers retrieval SNR by damping measurement signal, whereas an underestimated `RTAERR` destabilizes the SNR by allowing forward model noise to be interpreted as signal during retrieval. Here, we simply set `RTAERR` = 0 for all five experimental runs to avoid measurement damping for the sake of illustrating the CLIMCAPS HNO_3 retrieval approach. An operational configuration would require the accurate representation of `RTAERR` across the full IR spectrum to account for errors introduced by SARTA; however, previous experience suggests that the magnitude of `RTAERR` is very small and on the order of the instrument noise for most channels. The HNO_3 channel subset used in **R2**– **R5** employs all available CrIS channels in the ~11 μm band to maximize HNO_3 SNR (111 channels in total). Note that we avoid selecting channels from the two other HNO_3 absorption bands (Figure 1) because they are spectrally more complex, with multiple sources of interfering signals that manifest as geophysical noise in the retrieval. The IR window region, on the other hand, provides a strong SNR for stratospheric HNO_3 because the predominant source of geophysical noise is from the troposphere, which CLIMCAPS separates out ahead of the inversion step.

We varied `Bmax` in the **R2**, **R4** and **R5** experimental runs from low to high: 0.5, 2.5 and 10.0, respectively (Table 1). `Bmax` is a static scalar value that determines the eigenvalue threshold as $\lambda_c = \left[1/(\mathrm{Bmax})^2\right]$. Eigenvalues are a dimensionless quantity

https://doi.org/10.5194/egusphere-2025-1569
Preprint. Discussion started: 16 April 2025

that represents the HNO_3 SNR. CLIMCAPS uses λ_c in its regularization of the Bayesian inverse solution at run-time. A measurement eigenfunction is used without *any* damping (i.e., determined 100% in the retrieval) when its eigenvalue (λ_i) exceeds λ_c. In contrast, the eigenfunctions for which $\lambda_i < \lambda_c$ are either regularized (damped) or removed from the solution space altogether (filtered). The regularization factor, $\texttt{Rfac}_i$, determines how the eigenfunctions are treated as follows: $\texttt{Rfac}_i = \frac{\lambda_i}{(\lambda_i+\Delta\lambda)}$, where $\Delta\lambda = \sqrt{\lambda_c}\sqrt{\lambda_i} - \lambda_i$. When $0.05 < \texttt{Rfac}_i < 1.0$, the corresponding eigenfunction is damped anywhere between 0.01% to 95% as determined by the relation $100.0(1 - \texttt{Rfac}_i)$. All eigenfunctions for which $\texttt{Rfac}_i \leq 0.05$ are simply removed (or damped 100%) because the assumption is that these high-frequency eigenfunctions are dominated by noise relative to the target variable. In summary, a high `Bmax` corresponds to a low λ_c, which means that $\texttt{Rfac}_i$ will be higher overall with a larger set of eigenfunctions satisfying the conditions $\lambda_i > \lambda_c$. If `Bmax` is too low for a target variable, then the measurement signal may be overdamped such that the top eigenfunctions all have $\lambda_i \ll \lambda_c$. Conversely, if `Bmax` is too high, then measurement noise may be underdamped, with higher-order eigenfunctions – that contain mostly noise relative to the target variable – contributing to the solution. In such cases, the retrieval SNR is destabilized, which can result in retrievals that do not converge or AKs that are misshapen. We consider `Bmax` to be optimized for a target variable when it enables CLIMCAPS regularization to effectively function as a noise filter during run-time. It is worth emphasizing that these eigenfunctions represent the orthogonal vectors of the measurement error covariance matrix, $\mathbf{S}_m$, that CLIMCAPS calculates as the sum of the radiance error covariance, $\delta\mathbf{R}\delta\mathbf{R}^T$, and the uncertainty covariance for all background atmospheric state variables, $\sum \delta x_b x_b^T$ (Smith and Barnet, 2019). For the target variable HNO_3, this means that $\mathbf{S}_m$ is calculated as $\delta\mathbf{R}\delta\mathbf{R}^T + \delta x_{air\_temp} x_{air\_temp}^T + \delta x_{h2o\_vap} x_{h2o\_vap}^T + \delta x_{co2} x_{co2}^T + \delta x_{o3} x_{o3}^T + \delta x_{ch4} x_{ch4}^T + \delta x_{co} x_{co}^T + \delta x_{n2o} x_{n2o}^T$. We can contrast this against the theoretical OE approach put forward by Rodgers (2000) that regularizes the inverse solution with a generalized a priori error covariance $\mathbf{S}_a = \delta x_{\boldsymbol{hno3}} \delta x_{hno3}^T$ across all retrieval footprints irrespective of the variation in measurement information content. Note that we refer to the target variable as the a priori estimate, *a*, and all other state variables as background, *b*.

Table 2 illustrates how `Bmax` works in practice for seven profile retrievals – T_{air}, H_2O_{vap}, CO_2, O_3, CH_4, CO and HNO_3 – given the **R4** CLIMCAPS configuration. Tabulated like this, it becomes clear how the measurement signal for T_{air}, H_2O_{vap}, CO_2, O_3 and CH_4 is spread across multiple eigenfunctions and, in contrast, concentrated into a single dominant eigenfunction for CO and HNO_3. All eigenfunctions with `Rfac` values less than 5% are removed (filtered) from the solution space and thus treated as containing only noise relative to the a priori estimate. The measurement covariance matrix, $\mathbf{S}_m$, projected onto an orthogonal vector space like this captures the signal by the first few eigenfunctions, while the noise separates out into the remaining eigenfunctions. Looking more closely at H_2O_{vap}, we see that EF1 is fully determined in the retrieval (no damping), while EF2 is damped 55%, EF3 82%, EF4 87% and EF5 93%. It is different for T_{air}, for which EF1 through EF8 are all damped to some degree, with EF1 9% and EF8 95% as the extremes. When we look at O_3, we see by far the highest EF1 eigenvalue of all the variables listed. This can be explained by the fact that nadir-IR sounders have very strong sensitivity to stratospheric O_3 in the

https://doi.org/10.5194/egusphere-2025-1569
Preprint. Discussion started: 16 April 2025

1000–1100 cm^{-1} band (Figure 1) and almost negligible sensitivity to other background state variables in this spectral region. In addition to a high SNR for EF1, the O_3 EF2 and EF3 have eigenvalues that are relatively high as far as nadir-IR trace gas signals go, indicating the presence of a tropospheric O_3 signal. As demonstrated in Smith and Barnet (2020, 2024), the nadir-IR sounder sensitivity to tropospheric O_3 is high enough to warrant a profile product, which Gaudel et al. (2024) evaluated as part of the Tropospheric Ozone Assessment Report 2 (TOAR-II).

There is a direct relation between CLIMCAPS regularization and the retrieval AKs. Nothing illustrates this more clearly than the degrees of freedom for signal (DOFS). The DOFS of any Bayesian inverse solution can be calculated as the trace of the AK matrix (Rodgers, 2000) and are interpreted as the number of independent pieces of information in the measurement about a target variable. This can be a confusing concept to understand in the context of satellite soundings. What does it mean when we say that nadir-IR measurements typically have one DOFS for HNO_3? Table 2 illustrates what DOFS mean for CLIMCAPS retrievals, where the DOFS represent the sum of all $\mathtt{Rfac}_i$ values associated with the eigenfunction set used in determining the inverse solution. In other words, DOFS = 1.0 means that the equivalent of one eigenfunction determines the HNO_3 retrieval on all eight retrieval layers at a specific field-of-regard (FOR), or retrieval footprint. When DOFS < 1.0, it means that the HNO_3 eigenfunction needs to be damped ahead of retrieval to account for its low SNR.

Table 2: Eigenvalues and DOFS from an R4 run for seven retrieval variables – T_{air}, H_2O_{vap}, CO_2, CO, CH_4, O_3 and HNO_3 – at a single retrieval footprint. Row 1 reports the static Bmax threshold (and corresponding λ_c value) that CLIMCAPS employs at run-time to determine the degree of regularization for the Bayesian inverse solution. Row 2 details the eigenvalues (λ_i) and corresponding regularization factor, $\mathtt{Rfac}_i$, of the top eight eigenfunctions (EF1–EF8). All eigenvalues with $\mathtt{Rfac}_i$ < 5% are not considered in the retrieval (or damped 100%). The bottom row reports the DOFS calculated as the sum total of all $\mathtt{Rfac}_i$ values.

	T_{air}		H_2O_{vap}		CO_2		O_3		CH_4		CO		HNO_3	
Bmax	0.175		0.4		0.35		1.0		1.25		1.85		2.5	
λ_c	32.65		6.25		6,93		1.0		0.64		0.3		0.16	
	λ_i	Rfac	λ_i	Rfac	λ_i	Rfac	λ_i	Rfac	λ_i	Rfac	λ_i	Rfac	λ_i	Rfac
EF1	26.9	0.91	6.5	1.0	1.3	0.43	38.9	1.0	0.26	0.64	0.1	0.60	0.11	0.84
EF2	7.8	0.50	1.2	0.45	0.45	0.25	0.8	0.91	0.006	0.10	≪0.001	n/a	≪0.001	n/a
EF3	4.6	0.38	0.2	0.18	0.16	0.15	0.14	0.37	0.002	0.05	≪0.001	n/a	≪0.001	n/a
EF4	2.2	0.26	0.1	0.13	0.05	0.08	0.007	0.08	≪0.001	n/a	≪0.001	n/a	≪0.001	n/a
EF5	1.1	0.19	0.03	0.07	≪0.001	n/a	≪0.001	n/a	≪0.001	n/a	≪0.001	n/a	≪0.001	n/a
EF6	0.5	0.13	≪ 0.001	n/a	≪0.001	n/a	≪0.001	n/a	≪0.001	n/a	≪0.001	n/a	≪0.001	n/a
EF7	0.3	0.09	≪0.001	n/a	≪0.001	n/a	≪0.001	n/a	≪0.001	n/a	≪0.001	n/a	≪0.001	n/a
EF8	0.09	0.05	≪0.001	n/a	≪0.001	n/a	≪0.001	n/a	≪0.001	n/a	≪0.001	n/a	≪0.001	n/a
DOFS		**2.49**		**1.83**		**0.92**		**2.37**		**0.79**		**0.6**		**0.84**

Another mechanism CLIMCAPS employs to maximize the SNR for each target variable is channel selection. We calculate the statistical probability of each IR channel to observe the target variable offline using the method described in Gambacorta and

https://doi.org/10.5194/egusphere-2025-1569
Preprint. Discussion started: 16 April 2025

Barnet (2013). This means that the channel subsets are static across all FORs for a given product version (Smith and Barnet, 2024). However, future system upgrades can readily employ different channel subsets, so there is no requirement for the channel subsets to be fixed for all future versions of CLIMCAPS. In contrast, the degree to which the signal is captured (and noise is filtered) from the orthogonal measurement subset (eigenfunctions) is determined dynamically for each FOR at run-time. Given the changing climate, we consider this an important capability, especially for a multi-decadal product like CLIMCAPS, which cannot risk biasing its observational time-series with static assumptions about the a priori uncertainty.

CLIMCAPS retrieves cloud top pressure and cloud fraction, but only for the troposphere, so it does not have the ability to report on PSCs that initiate heterogeneous chemical processing in the polar stratosphere. Another factor to keep in mind is that CLIMCAPS performs "cloud clearing" on each cluster of 3 x 3 instrument fields-of-view (FOVs; ~15 km at nadir) and retrieves all geophysical variables on the aggregated FOR (~50 km at nadir). Cloud clearing uses spatial information to remove the spectral cloud signal from each measurement before inversion (Smith and Barnet 2023b), and it allows CLIMCAPS to quantify (and propagate) measurement error due to clouds in all atmospheric state retrievals. This not only helps stabilize the SNR, but also affords the ability to derive meaningful quality control (QC) metrics. One of the criteria in the CLIMCAPS QC flag is to reject retrievals with high error due to cloud contamination. All CLIMCAPS retrievals, therefore, represent the atmosphere around cloud fields, not inside them.

We ran CLIMCAPS on the JPSS-1 Level 1B files of CrIS and ATMS (Advanced Technology Microwave Sounder). We refer to the experimental configuration employed in this paper as CLIMCAPS-x to indicate that the results apply to all sounder configurations in general and to distinguish it from the operational implementation of CLIMCAPS V2.1 at the GES DISC. The Level 2 retrieval files report values on the nadir-IR sounder instrument grid. There are 45 scanlines per file, and each scanline spans nearly 2000 km with 30 FORs along track, such that the spatial resolution at nadir is ~50 km and at edge-of-scan ~150 km. These satellites orbit the Earth from pole to pole, so their wide swaths have significant overlap at high latitudes. A number of custom configurations for creating gridded Level 3 files are possible, depending on the target application. For the sake of illustration and clarity of argument, we aggregated the CLIMCAPS-x retrievals from all ascending JPSS-1 orbits (~1:30 pm local equator overpass time) onto 4° equal-angle global grids. Before aggregation, we vertically integrated the T_{air}, O_3 and HNO_3 profiles over all pressure layers in the 30–90 hPa range. Only those retrievals that passed CLIMCAPS QC were aggregated. We added DOFS to the suite of gridded variables to help interpret the results. CLIMCAPS QC is a simple "yes/no" flag derived from a large array of diagnostic metrics that includes errors due to cloud clearing, T_{air}, H_2O_{vap}, and cloud fraction. As our understanding of product applications matures, we envisage future CLIMCAPS upgrades to include customized QC metrics, especially for the trace gas species.

https://doi.org/10.5194/egusphere-2025-1569
Preprint. Discussion started: 16 April 2025

4 Results and Discussion

Having described the dynamic regularization mechanism of the CLIMCAPS inversion in Section 3, we now turn our attention to evaluating the five experimental runs, **R1**–**R5**. Figure 2 depicts the AKs (mean profile and standard deviation error bars) for all CLIMCAPS-x retrievals of T_{air}, O_3 and HNO_3 poleward of 40˚N latitude on 2 February 2020. The first point to note is that the T_{air} and O_3 AK profiles have error bars for more pressure layers than the HNO_3 AK. This is because nadir-IR sounders generally have higher information content for T_{air} and O_3 relative to that for HNO_3. CLIMCAPS, accordingly, has a unique set of trapezoidal pressure layers for each profile variable to allow the measurements to reliably map into retrieval space given the available information content. The higher the DOFS on average, the more retrieval layers are warranted. These retrieval layers are static across all FORs.

There are five HNO_3 AKs in Figure 2, corresponding to the five experimental runs. As mentioned, **R1** is closest to the CLIMCAPS V2.1 configuration, except that `RTAERR` = 0. The HNO_3 AKs for all five runs have peak sensitivity in the lower stratosphere, 30–90 hPa. We selected all available CrIS channels in the longwave IR window region (850–920 cm^{-1}) for the **R2**–**R5** CLIMCAPS-x runs to maximize measurement SNR for the sake of illustration. This is the same spectral region exploited for HNO_3 retrievals from GLORIA (Oelhaf et al., 2019) and IASI (Ronsmans et al., 2016). With everything else held constant, the only parameter that varies among **R2** (grey), **R3** (blue), **R4** (magenta) and **R5** (gold) is `Bmax`. It is, therefore, all the more remarkable to see how the corresponding HNO_3 AKs vary, not only in vertical structure, but also in their deviation about the mean in each effective pressure layer. **R2** registers the lowest values for HNO_3 AKs overall, and **R5** the highest. **R3** and **R4** result in AKs with similar vertical structure and variance, with **R4** having slightly higher AK values in the middle to upper troposphere.

In general, we know that IR sounder information content varies with ambient conditions, especially in the troposphere, where atmospheric variables have a large dynamic range in response to Earth surface and weather events (Smith and Barnet, 2019, 2020). So, we expect CLIMCAPS AKs to reflect this dynamic range with standard deviation error bars > 0.0. In general, Bayesian AKs with larger (smaller) peaks indicate an inverse solution with stronger (weaker) dependence on the measurement relative to the a priori estimate. In principle, AK = 0 indicates that the solution is the a priori estimate, and AK = 1.0 indicates that the solution is entirely measurement-based with no dependence on an a priori estimate. But measurements contain both signal *and* noise, so neither of these extremes manifest in reality. While a strong contribution from the measurement (sharply peaked AK) could be interpreted as preferable (e.g., to compensate for a priori uncertainty), one should always keep in mind that measurements contribute noise along with signal. So, a large AK value may very well indicate that the retrieval is dominated by measurement noise, not signal. This is why dynamic regularization of the inverse problem at run-time has proven to be such a robust mechanism for CLIMCAPS retrievals since the eigenvalue decomposition of each measurement SNR matrix helps filter noise. This simplifies error quantification during retrieval and minimizes the probability that retrievals are contaminated by measurement noise that is difficult to identify and quantify otherwise. Note that by “measurement noise”, we

https://doi.org/10.5194/egusphere-2025-1569
Preprint. Discussion started: 16 April 2025

do not simply mean the instrument error spectrum (or noise equivalent delta temperature, NEdT). Rather, measurement noise encapsulates all spectral information not directly related to a target variable. For example, the CrIS channels sensitive to mid-tropospheric CH_4 are also sensitive to mid-tropospheric H_2O_{vap} (Smith and Barnet, 2023a). If the target variable is CH_4, then H_2O_{vap} should be treated as geophysical noise, and vice versa. Smith and Barnet (2019) explain how we account for the many sources of measurement noise in CLIMCAPS.

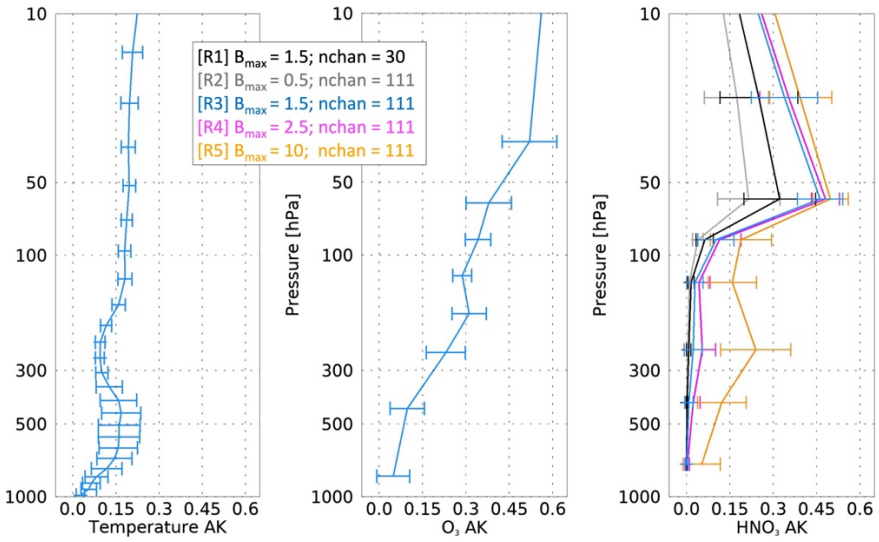

Figure 2: CLIMCAPS AK profiles for (left) T_{air}, (middle) O_3 and (right) HNO_3. These profiles represent the average of all diagonal elements from the AK matrices reported in the Level 2 product file for each retrieval parameter at every footprint poleward of 40°N latitude on 2 February 2020. The error bars represent the standard deviation of the AK profiles.

Table 3 tabulates the eigenvalues and regularization factor ($\texttt{Rfac}_i$) relative to HNO_3 for the first five eigenfunctions (EF1–EF5) of each experimental run. We report these values for two retrieval footprints independent of each other as well as the footprint represented in Table 2. `Bmax` determines the eigenvalue threshold, λ_c. In turn, $\texttt{Rfac}_i$ depends on the corresponding eigenvalue, λ_i, as well as λ_c. Table 3 illustrates the degree to which the HNO_3 eigenfunctions are regularized in the inverse solution at run-time. The EF2 eigenvalue is orders of magnitude smaller than the one for EF1, and all remaining eigenvalues (EF3–EF5) are roughly the same order of magnitude as EF2. As shown in Table 2, this is not the case for all CLIMCAPS retrieval variables. What it tells us is that most (if not all) of the signal for stratospheric HNO_3 compresses into a single eigenfunction that can readily be isolated from most (if not all) tropospheric signal and noise. With this table and associated discussion, we aim to illustrate how CLIMCAPS regularization works in practice and the things we consider when planning a system upgrade. The results presented in this paper help us identify which experimental configuration to adopt, test and refine for a future V3 public release. An in-depth quantification of the eigenfunctions across all retrieval footprints, and especially

https://doi.org/10.5194/egusphere-2025-1569
Preprint. Discussion started: 16 April 2025

the type of conditions of interest to seasonal monitoring in the extratropics, will be the focus of future work. Our objective here is simply to draw broad conclusions about each experimental configuration for the sake of identifying the path forward.

Table 3: A summary of the top five HNO_3 eigenvalues for two distinct retrieval footprints as processed by each experimental configuration, R1 – R5. The eigenfunctions of the radiance measurements are dependent on channel selection but independent of Bmax (λ_c). The latter is an empirical scalar that determines the degree to which CLIMCAPS regularizes Bayesian inverse solutions.

		R1 (λ_c = 0.16)		**R2** (λ_c = 4.0)		**R3** (λ_c = 0.44)		**R4** (λ_c = 0.16)		**R5** (λ_c = 0.01)	
		λ_i	Rfac	λ_i	Rfac	λ_i	Rfac	λ_i	Rfac	λ_i	Rfac
Footprint #1	EF1	0.01	0.15	0.16	0.20	0.22	0.70	0.34	1.0	0.33	1.0
	EF2	0.8E-05	n/a	0.1E-03	n/a	0.2E-03	n/a	0.4E-03	0.05	0.6E-04	0.08
	EF3	0.2E-05	n/a	0.2E-04	n/a	0.3E-04	n/a	0.4E-04	n/a	0.4E-04	0.06
	EF4	0.8E-06	n/a	0.1E-04	n/a	0.1E-04	n/a	0.3E-04	n/a	0.8E-05	n/a
	EF5	0.6E-06	n/a	0.3E-05	n/a	0.3E-05	n/a	0.1E-04	n/a	0.3E-05	n/a
		DOFS = 0.15		DOFS = 0.2		DOFS = 0.7		DOFS = 1.05		DOFS = 1.14	
Footprint #2	EF1	0.25	0.76	0.02	0.07	0.44	1.0	0.05	0.56	0.05	1.0
	EF2	0.7E-04	n/a	0.2E-04	n/a	0.2E-03	n/a	0.5E-04	n/a	0.5E-04	0.07
	EF3	0.1E-04	n/a	0.3E-05	n/a	0.4E-04	n/a	0.7E-05	n/a	0.7E-05	n/a
	EF4	0.9E-05	n/a	0.2E-05	n/a	0.1E-04	n/a	0.4E-05	n/a	0.4E-05	n/a
	EF5	0.5E-05	n/a	0.1E-05	n/a	0.1E-05	n/a	0.1E-05	n/a	0.1E-05	n/a
		DOFS = 0.76		DOFS = 0.07		DOFS = 1.0		DOFS = 0.56		DOFS = 1.07	

Comparison of the eigenvalues in Table 3 to the AK profiles in Figure 2 illuminates the observed differences. At the extremes are **R2** (Bmax = 0.5) and **R5** (Bmax = 10.0). The former harvests signal exclusively from the first eigenfunction in both cases, while the latter does so from two or more. This difference manifests in the **R2** AKs (grey) approaching zero in the troposphere, while the **R5** tropospheric AKs (gold) not only exceed 0.0 by a significant margin, but they also display a large dynamic range. Additionally, of all five runs, the **R2** AKs register the lowest values in the stratosphere overall. We attribute this to overdamping. With Bmax set to 0.5, **R2** has the highest threshold for determining whether an eigenfunction should be damped in the retrieval, with λ_c = 4.0. We have yet to observe a CLIMCAPS-x HNO_3 eigenvalue exceeding 4.0. This means that the first HNO_3 eigenfunction will always be damped in **R2**, irrespective of signal strength. Not only does λ_c determine which eigenfunctions to damp, it also determines the degree to which they are damped, such that the larger the difference between λ_c and λ_i, the smaller the $Rfac_i$ values, and the higher the degree of damping. **R2** illustrates how CLIMCAPS has the ability to overdamp nadir-IR measurements to the detriment of the inverse solution. Given that our objective with CLIMCAPS is to harvest as much of the available measurement signal as possible, while simultaneously accounting for most of the known sources of measurement noise, the value assigned to Bmax is an important consideration.

https://doi.org/10.5194/egusphere-2025-1569
Preprint. Discussion started: 16 April 2025

There is more to diagnose from the results presented in Table 3. **R5** has the highest Bmax (lowest λ_c) of all the runs, yet in the stratosphere its AKs approximate those from **R3** and **R4** (Figure 2). Moreover, irrespective of retrieval configuration, the HNO_3 AKs are always much smaller than 1.0, even at their peak around 50 hPa. We deduce that there must be an upper limit to the measurement signal for HNO_3, regardless of system parameters. In Table 3, we see that the eigenvalues of EF1 are always much less than 1.0, unlike those for T_{air}, H_2O_{vap}, O_3 and CO_2 (Table 2). This is because nadir-IR sensitivity to stratospheric HNO_3 is low even if the system is optimized.

When DOFS = 1.0, it means that the measurements contain one piece of information about the target variable. But this does not imply that one piece of measurement signal perfectly maps into one piece of atmospheric retrieval during inversion. For CLIMCAPS products, it simply means that the equivalent of one eigenvector determined the inverse solution in all pressure layers at a specific retrieval footprint. One can expand this argument as follows: The **R1**–**R3** configurations rarely have DOFS exceeding one. As seen in Figure 2, these are also the AKs with tropospheric values approaching zero. Only **R4** and **R5** have tropospheric AKs visibly greater than zero, and they are also the only two configurations often yielding DOFS > 1.0. This leads us to conclude that EF1 contains most of the available stratospheric signal for HNO_3, while EF2 and EF3 almost exclusively quantify tropospheric signal and noise. This clear distinction between EF1 and the other eigenfunctions is not the case for all retrieval variables. Table 2 illustrates that T_{air}, for example, depends on multiple eigenfunctions, all partially damped but none completely undamped. Wespes et al. (2007) reported that the DOFS of retrievals from IMG radiances range between 0.7 and 1.8 and concluded that this implied the ability of IMG measurements to provide two independent pieces of HNO_3 information – tropospheric and stratospheric partial columns. While a similar range is recorded for IASI HNO_3 DOFS (Ronsmans et al., 2016; Wespes et al., 2022), the retrievals are nonetheless presented as total column values. When a HNO_3 retrieval system, like FORLI, regularizes its Bayesian inversion along the full atmospheric column, without the ability to filter measurement noise at run-time, the stratospheric and tropospheric retrievals are correlated because their spectral SNR is correlated. A total column is, therefore, the only way to report such a retrieval to obtain a stable product. We argue that the CLIMCAPS approach to Bayesian inversion, on the other hand, benefits HNO_3 specifically because the stratospheric and tropospheric SNR can be decomposed into two separate eigenfunctions. This, of course, does not mean that it is the only Bayesian approach with the ability to distinguish an independent piece of stratospheric HNO_3 information. Compared to FORLI, however, CLIMCAPS has this novel capability.

Another aspect worth noting is that both **R1** and **R3** have Bmax = 1.5 (λ_c = 0.44), yet stratospheric **R1** AKs (Figure 2, black) are significantly smaller than those from **R3** (blue). This is due to the fact that the **R1** eigenfunctions are derived from 30 nadir-IR channels and those for **R3** from 111 channels. It is tempting, therefore, to conclude that this supports the use of all available channels during retrieval, but that would be an over-simplification. Figure 1 (as well as Figure 2 in Smith and Barnet, 2020) illustrates how nadir-IR measurements are highly mixed signals of multiple Earth system variables. We also know, empirically, that measurement SNR with respect to a target variable varies substantially because it depends on ambient conditions. One can enhance the effectiveness of CLIMCAPS regularization during inversion by pre-selecting measurement subsets with a high

https://doi.org/10.5194/egusphere-2025-1569
Preprint. Discussion started: 16 April 2025

probability of SNR > 1.0. This means selecting channels with high sensitivity and low geophysical noise (interference from background state variables) with respect to the target variable.

Figure 3 summarizes our discussion of DOFS for **R1** through **R5** with maps of the NH centred on the North Pole on 2 February 2020. The gridded average of DOFS, which we refer to as `avg`(DOFS) from here on, is displayed in the top row, with the standard deviation of the gridded DOFS, or `stdev`(DOFS), on the bottom. **R1** and **R3** yield similar spatial patterns for `avg`(DOFS) but different patterns for `stdev`(DOFS). With the **R1** eigenfunctions derived from 30 channels, unlike 111 in **R3**, it is possible that the smaller channel set lowers **R1** SNR to the point that its retrieval DOFS become unstable (i.e., highly variable). Given what we have learned from the values reported in Table 3, we argue that it is preferable for HNO_3 DOFS to approximate 1.0 – never to exceed it – and for EF1 to be fractionally damped only for the cases where the measurement SNR is low to begin with, such as where stratospheric HNO_3 concentrations are low. It is, therefore, interesting to compare **R3** and **R4**. Their `stdev`(DOFS) patterns are similar in that `stdev`(DOFS) is high wherever `avg`(DOFS) is low, despite the **R3** `avg`(DOFS) being much lower overall and **R4** `avg`(DOFS) approximating 1.0 across most of the study area. We can make sense of this when we revisit Tables 2 and 3, which show that $\texttt{Rfac}_i$ can have a large dynamic range – and thus high `stdev`(DOFS) – for small variations in all $\lambda_i < \lambda_c$. So even though **R3** may yield a relatively stable HNO_3 retrieval given its low `stdev`(DOFS) across most of the study region, its `avg`(DOFS) indicate that EF1, or the eigenfunction with most of the stratospheric HNO_3 signal, is probably overdamped. Of all five cases, we argue that **R4** yields the closest representation of what is needed for a stratospheric HNO_3 product aimed at science objectives related to ozone chemistry. In contrast, **R2** and **R5** epitomize what is *not* desirable in a stratospheric HNO_3 product, but for different reasons.

The maps in Figure 3 indicate that **R2** `stdev`(DOFS) is low wherever **R3** `stdev`(DOFS) is high (and vice versa), even though their `avg`(DOFS) maps show not dissimilar patterns. As discussed earlier, the **R2** configuration is associated with a very high λ_c, relatively speaking. And, the higher the λ_c, the larger the difference between λ_{EF1} and λ_c, leading, in turn, to a lower $\texttt{Rfac}_i$ and lower retrieval DOFS overall. In fact, the **R2** difference between λ_c and λ_{EF1} is so large that EF1 is always strongly damped, i.e., $\texttt{Rfac}_i$ is small and DOFS low. This is why the **R2** `avg`(DOFS) is overall significantly lower than that of all other configurations in Figure 3.

In contrast, **R5** `avg`(DOFS) exceeds 1.0 across the whole study area. This is not ideal because it means that the stratospheric HNO_3 retrieval is correlated with tropospheric noise. Two regions of the **R5** `stdev`(DOFS) map stand out as having values significantly higher than the background, namely the zones centred about (i) [40°–90°N, 50°–120° W], or the Siberian landmass, and (ii) [40°–60°N, 40°–160°E], which is North America. The Earth surface, boundary layer conditions and tropospheric weather processes are highly variable over land. When HNO_3 DOFS > 1.0, the measurement SNR for tropospheric conditions contributes to the retrieval as higher-order eigenfunctions that are damped anywhere between 0.01% to 95% according to $\texttt{Rfac}_i$. This leads us to conclude that it may be worth considering a customized HNO_3 configuration for future CLIMCAPS upgrades. For example, the `Rfac` of EF2 (and all higher-order eigenfunctions) can be set to a static value (≤ 0.05)

https://doi.org/10.5194/egusphere-2025-1569
Preprint. Discussion started: 16 April 2025

to always filter higher-order eigenfunctions, except EF1, to cap DOFS at 1.0 and thus isolate the stratospheric HNO_3 SNR. Of course, more research would need to be done to determine if such an approach is feasible under all conditions (i.e., demonstrate EF2 is always tropospheric), but CLIMCAPS could support such a customization in principle.

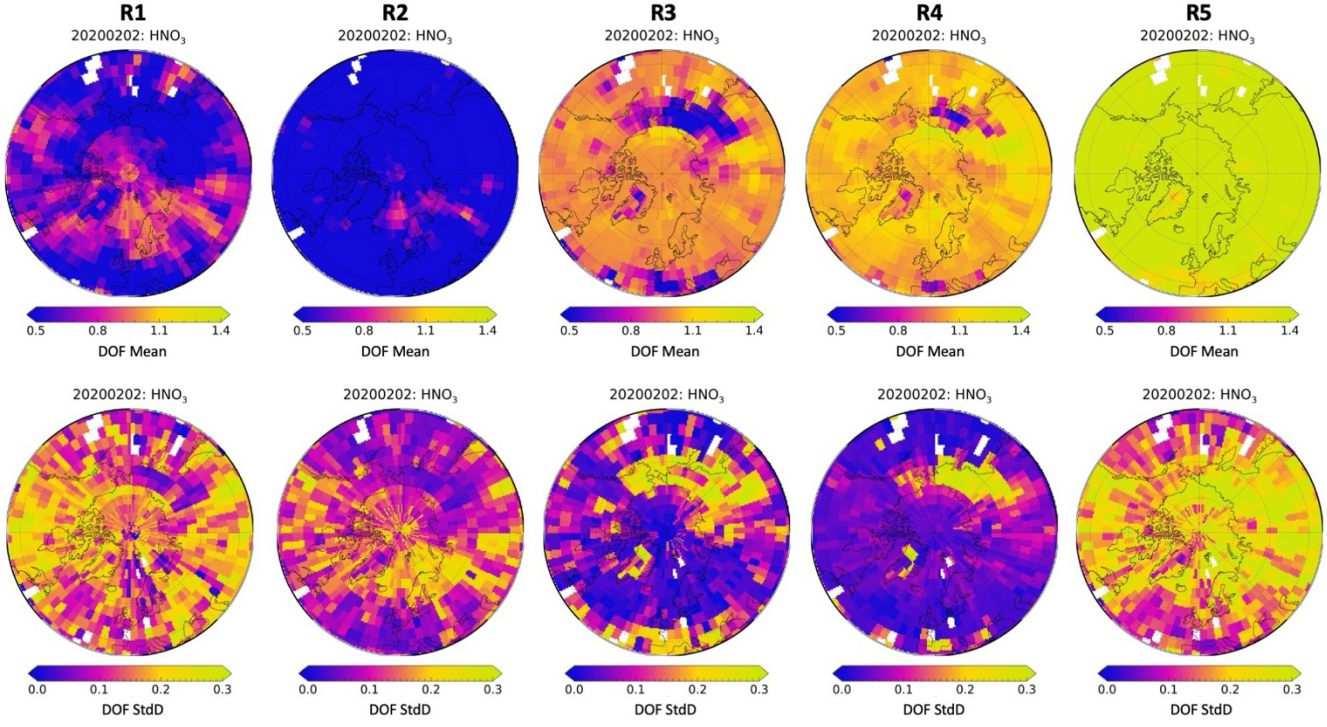

Figure 3: CLIMCAPS information content metrics (or, DOFS) aggregated onto a 4° equal-angle grid poleward of 40°N latitude. (Top row) Averaged HNO_3 DOFS. (Bottom row) Standard deviation of the HNO_3 DOFS. (Left to right) The five experimental setups as defined in Table 1.

We contrast the nadir-IR CLIMCAPS-x HNO_3 retrievals with those from limb-viewing MLS (V5, Livesey et al., 2022) in Figure 4 for five days spanning the Northern Hemisphere winter of 2019/2020. This figure depicts the formation and dissipation of an Arctic vortex as illustrated by the coincident CLIMCAPS-x retrievals of stratospheric T_{air} and O_3. We present CLIMCAPS-x V3 improvements for T_{air} and O_3 in a different paper (Smith and Barnet, 2024) and focus our discussion here on the contrast between MLS and CLIMCAPS retrievals of HNO_3. It is clear that MLS observes a much stronger HNO_3 spatial feature inside the Arctic vortex throughout the winter season. Compared to nadir sounders, limb sounders have the ability to observe stratospheric HNO_3 minima/maxima in much narrower pressure layers with greater sensitivity to small-scale changes. As seen in Figure 2, CLIMCAPS-x is sensitive to stratospheric HNO_3 across a single broad pressure layer. This reflects a fundamental limitation of nadir sounders. In fact, no matter how much we optimize the HNO_3 retrieval configuration, CLIMCAPS-x will never retrieve lower-stratospheric HNO_3 minima/maxima with the same accuracy as MLS. But absolute

https://doi.org/10.5194/egusphere-2025-1569
Preprint. Discussion started: 16 April 2025

accuracy is not the only metric that determines product value in applications. Often the spatial gradients themselves provide relevant information, as demonstrated in severe weather forecasting with gridded NUCAPS soundings (Berndt et al., 2020). Moreover, the day-to-day variations (relative changes) in HNO_3 abundances over the course of the season, as well as anomalies from a long-term climatology, might convey meaningful information even if the absolute magnitudes are wrong. Even though nadir-IR systems may be limited in the accuracy with which they can retrieve lower-stratospheric HNO_3 concentrations, they do provide a complete spatial representation day and night, through all seasons independent of sunlight. Future work could, therefore, focus on designing a custom HNO_3 gridded product with quality flags and a space-time aggregate configuration that clearly delineates the target features, such as the T_{air} product developed for aviation forecasts (Weaver et al., 2019). The applicability of CLIMCAPS-x HNO_3 could be significantly broadened in combination with coincident CLIMCAPS-x retrievals of stratospheric T_{air} and O_3.

It is worth taking a moment to reflect on the CLIMCAPS HNO_3 a priori estimate. At the core of any Bayesian inverse solution is its dependence on an a priori estimate. CLIMCAPS uses the AFGL climatology (Anderson et al., 1986) to define a static HNO_3 a priori estimate for retrievals at all footprints globally. While the AFGL climatology does not represent typical HNO_3 concentrations in the polar regions (it is orders of magnitude smaller than what MLS measures), it does benefit the CLIMCAPS-x HNO_3 product, given our target application of extratropical heterogeneous chemical processing in the lower stratosphere. It means that one can interpret the HNO_3 maps in Figure 4 as representing what the nadir sounders measure, not what the a priori estimate represents. Stated differently, CLIMCAPS-x depicts elevated HNO_3 values (i.e., retrieval > a priori estimate) only where the nadir measurements have sensitivity to HNO_3 due to measurable concentrations in the lower stratosphere. Conversely, the CLIMCAPS-x HNO_3 retrieval approximates the a priori estimate wherever stratospheric HNO_3 concentrations are too low to be measurable by the nadir-IR sounders. While such an atypical a priori estimate may contribute to a slower rate of convergence during Bayesian inversion, it does not significantly impact the CLIMCAPS-x retrieval, which routinely logs rapid convergence (2–3 iterations) to a stable solution. The result is a retrieval product that depicts HNO_3 spatial patterns as a function of nadir sounder observing capability.

https://doi.org/10.5194/egusphere-2025-1569
Preprint. Discussion started: 16 April 2025

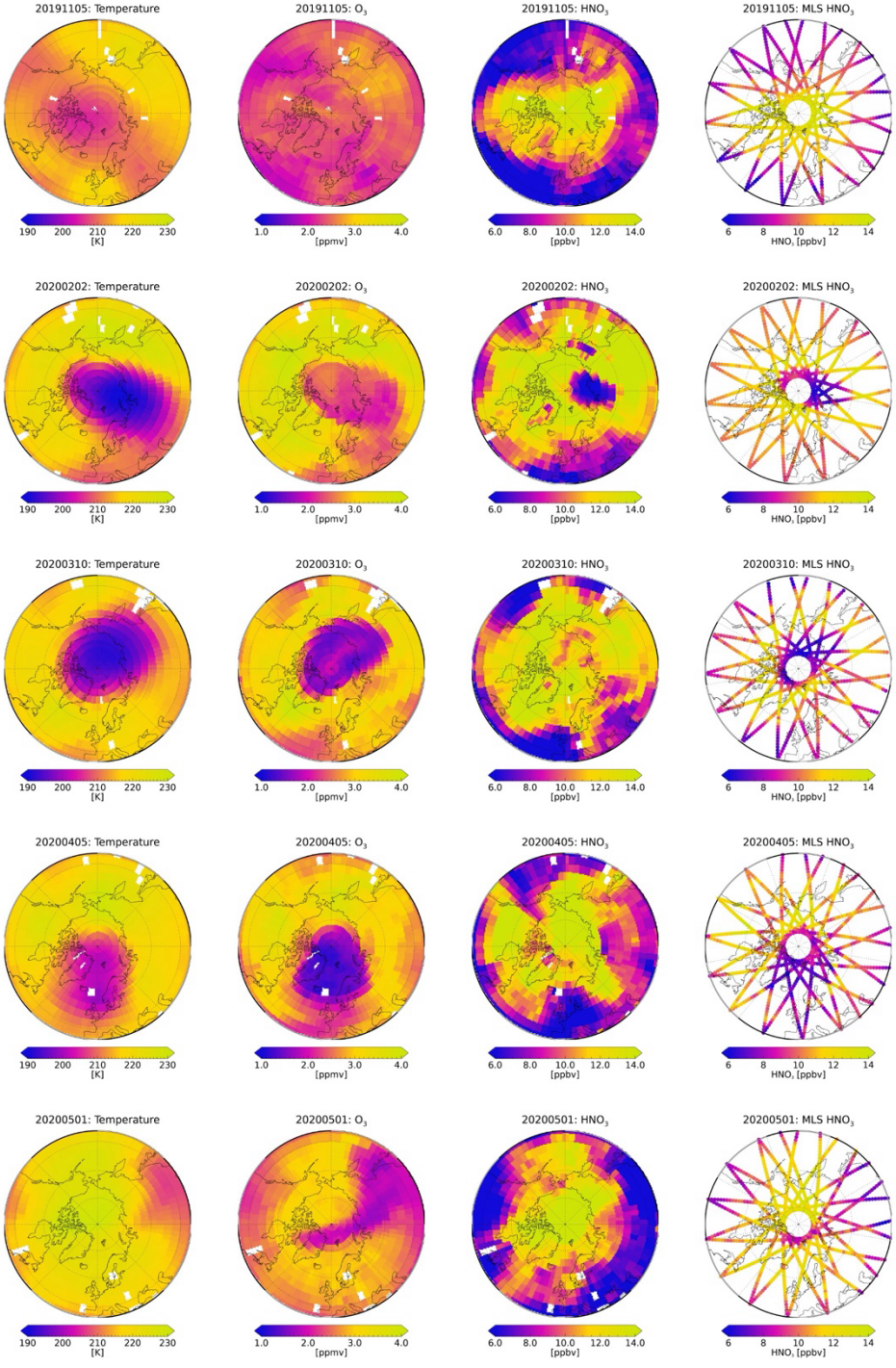

Figure 4: A time series of lower stratospheric (30–90 hPa) CLIMCAPS-x retrievals of T_{air}, O_3, and HNO_3 aggregated onto a 4° equal-angle grid throughout the 2019/2020 Northern Hemisphere winter season poleward of 40°N latitude. The column on the right represents the MLS V5 Level 2 HNO_3 retrievals.

https://doi.org/10.5194/egusphere-2025-1569
Preprint. Discussion started: 16 April 2025

The CLIMCAPS-x retrievals of T_{air}, H_2O_{vap} and O_3 need to serve a broader range of scientific foci with more accurate estimates of absolute quantities, so for those variables Smith and Barnet (2019, 2020) instead implemented as a priori estimate a reanalysis model, specifically, the Modern-era Retrospective analysis for Research and Applications (MERRA-2; Gelaro et al., 2017). In future, and as our knowledge of product applications evolves, we can test the sensitivity of CLIMCAPS-x HNO_3 retrievals to different a priori estimates, such as zonal estimates based on MLS retrievals or the FORLI HNO_3 a priori estimate, which is an aggregate profile derived from chemistry transport model fields and other retrieval systems (Hurtmans et al., 2012).

5 Conclusions

Nadir-IR measurements, like those from AIRS, CrIS and IASI, are predominantly sensitive to lower stratospheric (30–90 hPa) HNO_3 in the ~11 μm window region (850–920 cm^{-1}) of their longwave IR bands. This paper provides a progress report on the development of CLIMCAPS HNO_3 retrievals and shows that the resulting HNO_3 product generally reflects real atmospheric variations. We demonstrated how the CLIMCAPS retrieval approach allows its HNO_3 product to be reported as a partial stratospheric column that is largely independent of tropospheric noise. The FORLI product, in contrast, reports HNO_3 retrievals as total column quantities (i.e., integrated over all pressure layers from the Earth surface to the TOA) because their stratospheric and tropospheric HNO_3 retrievals are correlated. Future work will focus on quantifying HNO_3 product differences between CLIMCAPS (from AIRS and CrIS) and FORLI (from IASI) in their characterization of the day-to-day variation of the extratropical stratosphere. The goal of this paper was to report on the degree to which the operational CLIMCAPS V2.1 HNO_3 product can be improved to allow for such a comparison so that nadir-IR HNO_3 products may prove useful in filling the data gap when Aura is decommissioned in the next few years. Nadir-IR products alone cannot match or replace the limb-viewing MLS observing capability, but, paired with those from OMPS/LP, could help monitor polar processes with an HNO_3 product indicating polar stratospheric cloud (PSC) formation irrespective of sunlight.

The first of two objectives was to test the sensitivity of the CLIMCAPS HNO_3 retrieval to two algorithm components, namely channel selection and Bayesian regularization. To this end, our results indicate that the HNO_3 SNR stabilizes significantly when all channels in the ~11 μm window region are employed. Additionally, the CLIMCAPS HNO_3 retrieval is highly sensitive to variations in `Bmax` – a scalar that determines the eigenvalue threshold, λ_c, employed at run-time to regularize the inverse solution according to the information content available in each cloud-cleared measurement. We gave a generalized overview of this component of the CLIMCAPS retrieval approach and illustrated the importance of optimizing `Bmax` for each retrieval parameter individually.

The second objective was to determine whether nadir-IR measurements allow the stable retrieval (and independent reporting) of stratospheric HNO_3. Currently, the state-of-the-art nadir-IR system, namely FORLI, report its HNO_3 retrieval as a total column product to account for pressure-dependent correlations. A stand-alone stratospheric HNO_3 product would, therefore, be a marked improvement and one that, we argue, is necessary given the impending loss of MLS measurements when the Aura platform is decommissioned. We determined that most of the CrIS spectral information content for stratospheric HNO_3

https://doi.org/10.5194/egusphere-2025-1569
Preprint. Discussion started: 16 April 2025

compresses into a unique eigenfunction that we can isolate from all the remaining eigenfunctions using the dynamic regularization mechanism in CLIMCAPS. Overall, the experiments reported here clarified the steps we need to take to upgrade the CLIMCAPS HNO_3 product in a future release.

Acknowledgements

We would like to acknowledge that NOAA, and specifically Walter Wolf, supported the development of the HNO_3 retrieval code during NUCAPS algorithm development, circa 2003 to 2008. Without this support it would have been extremely difficult to retrofit the infrastructure necessary to add the product at a later date, and it would have been prohibitive to perform the work discussed in this paper under the NASA ROSES maintenance funding alone (ROSES grant no. 80NSSC21K1959). We also acknowledge Fengying Sun for a number of early studies to optimize the HNO_3 retrieval step for use within the operational NUCAPS configuration. During the development of CLIMCAPS (2018–2020), we were able to leverage more than a decade of experience within NOAA. Work at the Jet Propulsion Laboratory, California Institute of Technology, was carried out under a contract with NASA (no. 80NM0018D0004).

Competing interests

The contact author has declared that none of the authors has any competing interests.

Author contribution

NS conceptualized this work and designed the experiments. CB is the architect and developer of the CLIMCAPS software. NS performed the formal analysis and generated all graphics. MLS and CB reviewed the study and provided critical input that guided the analysis and interpretation of results. NS wrote the original draft, with MLS and CB both reviewing the manuscript before submission.

Data Availability

The CLIMCAPS V2.1 L2 retrieval product is archived at and distributed by the NASA GES DISC for Aqua (2002–2016; Smith, 2019a), SNPP (2016–2018; Smith, 2019c) and JPSS-1 (2018–present; Smith, 2019b). We additionally employed the MLS/Aura HNO_3 V005 Level 2 product also archived at GES DISC (Manney et al., 2020).

References

Anderson, G. P., Clough, S. A., Kneizys, F. X., Chetwynd, J. H., and Shettle, E. P.: Air Force Geophysical Laboratory (AFGL) atmospheric constituent profiles, U. S. Department of Commerce, 1986.

Aumann, H. H., Chahine, M. T., Gautier, C., Goldberg, M. D., Kalnay, E., McMillin, L. M., Revercomb, H., Rosenkranz, P. W., Smith, W. L., Staelin, D. H., Strow, L. L., and Susskind, J.: AIRS/AMSU/HSB on the aqua mission: design, science

https://doi.org/10.5194/egusphere-2025-1569
Preprint. Discussion started: 16 April 2025

objectives, data products, and processing systems, IEEE Transactions on Geoscience and Remote Sensing, 41, 253–264, https://doi.org/10.1109/TGRS.2002.808356, 2003.

Barnet, C. D., Divakarla, M., Gambacorta, A., Iturbide-Sanchez, F., Tan, C., Wang, T., Warner, J., Zhang, K., and Zhu, T.: NOAA Unique Combined Atmospheric Processing System (NUCAPS) algorithm theoretical basis document, National Oceanic and Atmospheric Administration, Washington, D. C., USA, https://www.star.nesdis.noaa.gov/jpss/documents/ATBD/ATBD_NUCAPS_v3.1.pdf (last access: 4 April 2025), 2021.

Berndt, E. B., Smith, N., Burks, J., White, K., Esmaili, R., Kuciauskas, A., Duran, E., Allen, R., LaFontaine, F., and Szkodzinski, J.: Gridded Satellite Sounding Retrievals in Operational Weather Forecasting: Product Description and Emerging Applications, Remote Sensing, 12, 3311, https://doi.org/10.3390/rs12203311, 2020.

Berndt, E. B., Smith, N., and Barnet, C. D.: Integrating NASA Aqua AIRS in a Real-Time NUCAPS Science-To-Applications System to Support Severe Weather Forecasting, Earth and Space Science, 10, e2022EA002725, https://doi.org/10.1029/2022EA002725, 2023.

Brakebusch, M., Randall, C. E., Kinnison, D. E., Tilmes, S., Santee, M. L., and Manney, G. L.: Evaluation of Whole Atmosphere Community Climate Model simulations of ozone during Arctic winter 2004–2005, JGR Atmospheres, 118, 2673–2688, https://doi.org/10.1002/jgrd.50226, 2013.

Chalon, G., Astruc, P., Hébert, Ph., Blumstein, D., Buil, C., Carlier, T., Clauss, A., Siméoni, D., and Tournier, B.: IASI instrument: technical description and measured performances, in: International Conference on Space Optics — ICSO 2004, International Conference on Space Optics 2004, Toulouse, France, 51, https://doi.org/10.1117/12.2308007, 2017.

Flynn, L. E., Seftor, C. J., Larsen, J. C., and Xu, P.: The Ozone Mapping and Profiler Suite, in: Earth Science Satellite Remote Sensing, edited by: Qu, J. J., Gao, W., Kafatos, M., Murphy, R. E., and Salomonson, V. V., Springer Berlin Heidelberg, Berlin, Heidelberg, 279–296, https://doi.org/10.1007/978-3-540-37293-6_15, 2006.

Gambacorta, A. and Barnet, C. D.: Methodology and information content of the NOAA NESDIS operational channel selection for the Cross-Track Infrared Sounder (CrIS), IEEE T. Geosci. Remote, 51, 3207–3216, https://doi.org/10.1109/TGRS.2012.2220369, 2013.

Gaudel, A., Bourgeois, I., Li, M., Chang, K.-L., Ziemke, J., Sauvage, B., Stauffer, R. M., Thompson, A. M., Kollonige, D. E., Smith, N., Hubert, D., Keppens, A., Cuesta, J., Heue, K.-P., Veefkind, P., Aikin, K., Peischl, J., Thompson, C. R., Ryerson, T. B., Frost, G. J., McDonald, B. C., and Cooper, O. R.: Tropical tropospheric ozone distribution and trends from in situ and satellite data, Atmos. Chem. Phys., 24, 9975–10000, https://doi.org/10.5194/acp-24-9975-2024, 2024.

Gelaro, R., McCarty, W., Suárez, M. J., Todling, R., Molod, A., Takacs, L., Randles, C. A., Darmenov, A., Bosilovich, M. G., Reichle, R., Wargan, K., Coy, L., Cullather, R., Draper, C., Akella, S., Buchard, V., Conaty, A., da Silva, A. M., Gu, W., Kim, G.-K., Koster, R., Lucchesi, R., Merkova, D., Nielsen, J. E., Partyka, G., Pawson, S., Putman, W., Rienecker, M., Schubert, S. D., Sienkiewicz, M., and Zhao, B.: The modern-era retrospective analysis for research and applications, Version 2 (MERRA-2), J. Climate, 30, 5419–5454, https://doi.org/10.1175/JCLI-D-16-0758.1, 2017.

Glumb, R. J., Jordan, D. C., and Mantica, P.: Development of the Crosstrack Infrared Sounder (CrIS) sensor design, SPIE 4486, Infrared Spaceborne Remote Sensing IX, International Symposium on Optical Science and Technology, San Diego, CA, 29 July–3 August 2001, SPIE, 411–424, https://doi.org/10.1117/12.455124, 2002.

Hurtmans, D., Coheur, P.-F., Wespes, C., Clarisse, L., Scharf, O., Clerbaux, C., Hadji-Lazaro, J., George, M., and Turquety, S.: FORLI radiative transfer and retrieval code for IASI, Journal of Quantitative Spectroscopy and Radiative Transfer, 113, 1391–1408, https://doi.org/10.1016/j.jqsrt.2012.02.036, 2012.

https://doi.org/10.5194/egusphere-2025-1569
Preprint. Discussion started: 16 April 2025

Lambert, A., Santee, M. L., and Livesey, N. J.: Interannual variations of early winter Antarctic polar stratospheric cloud formation and nitric acid observed by CALIOP and MLS, Atmos. Chem. Phys., 16, 15219–15246, https://doi.org/10.5194/acp-16-15219-2016, 2016.

Livesey, N. J., Read, W. G., Wagner, P. A., Froidevaux, L., Santee, M. L., and Schwartz, M. J. et al.: Version 5.0x Level 2 and 3 data quality and description document, (Tech. Rep. No. JPL D-105336 Rev. B). Jet Propulsion Laboratory, https://mls.jpl.nasa.gov/data/v5-0_data_quality_document.pdf (last access: 4 April 2025), 2022.

Maddy, E. S. and Barnet, C. D.: Vertical resolution estimates in Version 5 of AIRS operational retrievals, IEEE T. Geosci. Remote, 46, 2375–2384, https://doi.org/10.1109/TGRS.2008.917498, 2008.

Manney, G. L., Santee, M. L., Froidevaux, L., Livesey, N., and Read, W.: MLS/Aura Level 2 Nitric Acid (HNO3) Mixing Ratio V005. [Dataset], Goddard Earth Sciences Data and Information Services Center (GES DISC). https://doi.org/10.5067/AURA/MLS/DATA2511, 2020.

Murphy, D. M. and Gary, B. L.: Mesoscale Temperature Fluctuations and Polar Stratospheric Clouds, J. Atmos. Sci., 52, 1753–1760, https://doi.org/10.1175/1520-0469(1995)052<1753:MTFAPS>2.0.CO;2, 1995.

Oelhaf, H., Sinnhuber, B.-M., Woiwode, W., Bönisch, H., Bozem, H., Engel, A., Fix, A., Friedl-Vallon, F., Grooß, J.-U., Hoor, P., Johansson, S., Jurkat-Witschas, T., Kaufmann, S., Krämer, M., Krause, J., Kretschmer, E., Lörks, D., Marsing, A., Orphal, J., Pfeilsticker, K., Pitts, M., Poole, L., Preusse, P., Rapp, M., Riese, M., Rolf, C., Ungermann, J., Voigt, C., Volk, C. M., Wirth, M., Zahn, A., and Ziereis, H.: POLSTRACC: Airborne Experiment for Studying the Polar Stratosphere in a Changing Climate with the High Altitude and Long Range Research Aircraft (HALO), BAMS, 100, 2634–2664, https://doi.org/10.1175/BAMS-D-18-0181.1, 2019.

Pagano, T. S., Aumann, H. H., Hagan, D. E., and Overoye, K.: Prelaunch and in-flight radiometric calibration of the atmospheric infrared sounder (AIRS), IEEE T. Geosci. Remote, 41, 265–273, https://doi.org/10.1109/TGRS.2002.808324, 2003.

Ronsmans, G., Langerock, B., Wespes, C., Hannigan, J. W., Hase, F., Kerzenmacher, T., Mahieu, E., Schneider, M., Smale, D., Hurtmans, D., De Mazière, M., Clerbaux, C., and Coheur, P.-F.: First characterization and validation of FORLI-HNO3 vertical profiles retrieved from IASI/Metop, Atmos. Meas. Tech., 9, 4783–4801, https://doi.org/10.5194/amt-9-4783-2016, 2016.

Ronsmans, G., Wespes, C., Hurtmans, D., Clerbaux, C., and Coheur, P.-F.: Spatio-temporal variations of nitric acid total columns from 9 years of IASI measurements – a driver study, Atmos. Chem. Phys., 18, 4403–4423, https://doi.org/10.5194/acp-18-4403-2018, 2018.

Santee, M. L., MacKenzie, I. A., Manney, G. L., Chipperfield, M. P., Bernath, P. F., Walker, K. A., Boone, C. D., Froidevaux, L., Livesey, N. J., and Waters, J. W.: A study of stratospheric chlorine partitioning based on new satellite measurements and modeling, J. Geophys. Res., 113, D12307, https://doi.org/10.1029/2007JD009057, 2008.

Smith, N: Sounder SIPS Aqua AIRS IR + MW Level 2 CLIMCAPS retrieved atmospheric state V2.1 [Dataset]. https://doi.org/10.5067/J7GVFM11OGIX, 2019a.

Smith, N: Sounder SIPS JPSS-1 CrIMSS Level 2 CLIMCAPS retrieved atmospheric state V2.1 [Dataset]. https://doi.org/10.5067/5GHJWKUXQSP6, 2019b.

Smith, N: Sounder SIPS Suomi NPP CrIMSS Level 2 CLIMCAPS Full Spectral Resolution retrieved atmospheric state V2.1 [Dataset]. https://doi.org/10.5067/SD6WORV4GX8P, 2019c.

https://doi.org/10.5194/egusphere-2025-1569
Preprint. Discussion started: 16 April 2025

Smith, N. and Barnet, C. D.: Uncertainty Characterization and Propagation in the Community Long-Term Infrared Microwave Combined Atmospheric Product System (CLIMCAPS), Remote Sensing, 11, 1227, https://doi.org/10.3390/rs11101227, 2019.

Smith, N. and Barnet, C. D.: CLIMCAPS observing capability for temperature, moisture, and trace gases from AIRS/AMSU and CrIS/ATMS, Atmos. Meas. Tech., 13, 4437–4459, https://doi.org/10.5194/amt-13-4437-2020, 2020.

Smith, N. and Barnet, C. D.: CLIMCAPS—A NASA Long-Term Product for Infrared + Microwave Atmospheric Soundings, Earth and Space Science, 10, e2022EA002701, https://doi.org/10.1029/2022EA002701, 2023a.

Smith, N. and Barnet, C. D.: Practical Implications of CLIMCAPS Cloud Clearing and Derived Quality Metrics, Earth and Space Science, 10, e2023EA002913, https://doi.org/10.1029/2023EA002913, 2023b.

Smith, N. and Barnet, C. D.: An information content approach to diagnosing and improving CLIMCAPS retrievals across instruments and satellites, https://doi.org/10.5194/egusphere-2024-2448, 2024.

Solomon, S.: Stratospheric ozone depletion: a review of concepts and history, Reviews of Geophysics, 37, 275–316, https://doi.org/10.1029/1999RG900008, 1999.

Strow, L. L., Hannon, S. E., De Souza-Machado, S., Motteler, H. E., and Tobin, D.: An overview of the AIRS radiative transfer model, IEEE T. Geosci. Remote, 41, 303–313, https://doi.org/10.1109/TGRS.2002.808244, 2003.

Strow, L. L., Motteler, H., Tobin, D., Revercomb, H., Hannon, S., Buijs, H., Predina, J., Suwinski, L., and Glumb, R.: Spectral calibration and validation of the Cross-track Infrared Sounder on the Suomi NPP satellite: CrIS spectral calibration, J. Geophys. Res., 118, 12,486-12,496, https://doi.org/10.1002/2013JD020480, 2013.

Susskind, J., Barnet, C. D., and Blaisdell, J. M.: Retrieval of atmospheric and surface parameters from AIRS/AMSU/HSB data in the presence of clouds, IEEE T. Geosci. Remote, https://doi.org/10.1109/TGRS.2002.808236, 41, 390–409, 2003.

Toon, O. B., Hamill, P., Turco, R. P., and Pinto, J.: Condensation of HNO3 and HCl in the winter polar stratospheres, Geophys. Res. Lett., 13, 1284–1287, https://doi.org/10.1029/GL013i012p01284, 1986.

Tritscher, I., Pitts, M. C., Poole, L. R., Alexander, S. P., Cairo, F., Chipperfield, M. P., Grooß, J., Höpfner, M., Lambert, A., Luo, B., Molleker, S., Orr, A., Salawitch, R., Snels, M., Spang, R., Woiwode, W., and Peter, T.: Polar Stratospheric Clouds: Satellite Observations, Processes, and Role in Ozone Depletion, Reviews of Geophysics, 59, e2020RG000702, https://doi.org/10.1029/2020RG000702, 2021.

Wargan, K., Kramarova, N., Weir, B., Pawson, S., and Davis, S. M.: Toward a Reanalysis of Stratospheric Ozone for Trend Studies: Assimilation of the Aura Microwave Limb Sounder and Ozone Mapping and Profiler Suite Limb Profiler Data, J. Geophys. Res., 125, e2019JD031892, https://doi.org/10.1029/2019JD031892, 2020.

Waters, J. W., Froidevaux, L., Harwood, R. S., Jarnot, R. F., Pickett, H. M., Read, W. G., Siegel, P. H., Cofield, R. E., Filipiak, M. J., Flower, D. A., Holden, J. R., Lau, G. K., Livesey, N. J., Manney, G. L., Pumphrey, H. C., Santee, M. L., Wu, D. L., Cuddy, D. T., Lay, R. R., Loo, M. S., Perun, V. S., Schwartz, M. J., Stek, P. C., Thurstans, R. P., Boyles, M. A., Chandra, K. M., Chavez, M. C., Gun-Shing Chen, Chudasama, B. V., Dodge, R., Fuller, R. A., Girard, M. A., Jiang, J. H., Yibo Jiang, Knosp, B. W., LaBelle, R. C., Lam, J. C., Lee, K. A., Miller, D., Oswald, J. E., Patel, N. C., Pukala, D. M., Quintero, O., Scaff, D. M., Van Snyder, W., Tope, M. C., Wagner, P. A., and Walch, M. J.: The Earth observing system microwave limb sounder (EOS MLS) on the aura Satellite, IEEE T. Geosci. Remote, 44, 1075–1092, https://doi.org/10.1109/TGRS.2006.873771, 2006.

Weaver, G., Smith, N., Berndt, E. B., White, K. D., Dostalek, J. F., and Zavodsky, B. T.: Addressing the cold air aloft aviation challenge with satellite sounding observations, J. Oper. Meteor., 138–152, https://doi.org/10.15191/nwajom.2019.0710, 2019.

https://doi.org/10.5194/egusphere-2025-1569
Preprint. Discussion started: 16 April 2025

Wespes, C., Hurtmans, D., Herbin, H., Barret, B., Turquety, S., Hadji-Lazaro, J., Clerbaux, C., and Coheur, P.: First global distributions of nitric acid in the troposphere and the stratosphere derived from infrared satellite measurements, J. Geophys. Res., 112, 2006JD008202, https://doi.org/10.1029/2006JD008202, 2007.

Wespes, C., Hurtmans, D., Clerbaux, C., Santee, M. L., Martin, R. V., and Coheur, P. F.: Global distributions of nitric acid from IASI/MetOP measurements, Atmos. Chem. Phys., 9, 7949–7962, https://doi.org/10.5194/acp-9-7949-2009, 2009.

Wespes, C., Ronsmans, G., Clarisse, L., Solomon, S., Hurtmans, D., Clerbaux, C., and Coheur, P.-F.: Polar stratospheric nitric acid depletion surveyed from a decadal dataset of IASI total columns, Atmos. Chem. Phys., 22, 10993–11007, https://doi.org/10.5194/acp-22-10993-2022, 2022.